J. Fluid Mech. (1990), *vol.* 221, *pp.* 105–129
Printed in Great Britain

Linear stability of natural convection in spherical annuli

By DAVID R. GARDNER,[1] ROD W. DOUGLASS[2] AND STEVEN A. TROGDON[3]

[1] Nuclear Energy Science and Materials Technology, Severe Accident Phenomenology Division, Sandia National Laboratories, Albuquerque, NM 87185-5800, USA

[2] Computational Mechanics Laboratory, Department of Mechanical Engineering, University of Nebraska-Lincoln, Lincoln, NE 68588-0656, USA

[3] Department of Mathematics and Statistics, University of Minnesota-Duluth, Duluth, MN 55812-2496, USA

(Received 13 February 1989 and in revised form 1 May 1990)

Natural convection in a Boussinesq fluid filling the narrow gap between two isothermal, concentric spheres at different temperatures depends strongly on radius ratio, Prandtl number, and Grashof number. When the inner sphere has a higher temperature than the outer sphere, and for fixed values of radius ratio and Prandtl number, experiments show the flow to be steady and axisymmetric for sufficiently small Grashof number and quasi-periodic and axisymmetric for Grashof numbers greater than a critical value. It is our hypothesis that the observed transition is a flow bifurcation. This hypothesis is examined by solving an appropriate eigenvalue problem. The critical Grashof number, critical eigenvalues, and corresponding eigenvectors are obtained as functions of the radius ratio, Prandtl number, and longitudinal wavenumber. Critical Grashof numbers range from 1.18×10^4 to 2.63×10^3 as Prandtl number Pr increases from zero to 0.7, for radius ratios of 0.900 and 0.950. A transitional Prandtl number Pr_t exists such that for $Pr < Pr_t$ the bifurcation is time-periodic and axisymmetric. For $Pr > Pr_t$ the bifurcation is steady and non-axisymmetric with wavenumber two.

A first approximation to the bifurcated flow is obtained using the critical eigenvectors. For $Pr < Pr_t$ the bifurcation sets in as a cluster of relatively strong cells with alternating directions of rotation. The cells remain fixed in location, but pulsate with time. The cluster moves toward the top of the annulus as Pr increases toward Pr_t. An important feature of the non-axisymmetric bifurcation for $Pr > Pr_t$ is a set of four cells located at each pole of the annulus in which the radial velocity alternates direction in moving from any one cell to an adjacent one. For fixed radius ratio, the average Nusselt number at criticality varies only slightly with Prandtl number.

1. Introduction

The objective of the work reported here is to investigate the linear stability and bifurcation of the natural convection flow of a viscous fluid contained in a narrow-gap, concentric spherical annulus, using an appropriate numerical model. The two spherical shells are isothermal, and the temperature of the inner sphere is greater than that of the outer sphere. The resulting basic motion is assumed to be steady, axisymmetric, and isochoric. Disturbances to the basic motion are fully three-dimensional and time-dependent. In this problem, gravity acts everywhere parallel to a fixed vertical axis of the annulus. This problem is thus different from the

spherical analogue of the Rayleigh–Bénard problem, in which gravity acts radially inward, and consequently the basic motion is quiescent: for a temperature difference between the spherical shells below a critical value the fluid between the spheres is at rest. In the problem addressed here, there is a non-quiescent basic motion for all non-zero temperature differences between the bounding spheres.

This problem is motivated by the experimental observations of several researchers, notably Bishop *et al.* (1964*a*, *b*), Bishop, Mack & Scanlon (1966) and Yin *et al.* (1973), who produced the first flow visualization data for this problem; air and water were the working fluids. These observations reveal certain regularities of behaviour in which, for a given fluid, the flow pattern observed depends on the width of the gap and the temperature difference between the spheres. For most fluids, a steady, axisymmetric motion is induced by buoyancy forces as the temperature difference between the spheres is increased from zero. As the temperature difference is increased, this basic motion adjusts to the increased driving potential primarily by increasing fluid velocity. At a critical temperature difference, which depends on the gap width and Prandtl number, the basic motion becomes unstable to small disturbances and bifurcates to another, distinctly different, stable flow pattern, which may be unsteady and non-axisymmetric.

The problem of computing the natural convection basic motion has been addressed in a number of studies which began with the transient finite-difference solution of Brown (1967). Over the subsequent twenty years the problem has been solved by a variety of methods for a variety of fluids and geometries (e.g. Mack & Hardee 1968; Singh & Chen 1980; Astill, Leong & Martorana 1980; Caltagirone, Combarnous & Mojtabi 1980; Ingham 1981; Singh & Elliot 1981; Nelsen, Douglass & Alexander 1982; Mojtabi & Caltagirone 1982; Nelsen & Douglass 1984; and Wright & Douglass 1986). Certain conclusions emerge from an examination of this body of work. First, all the studies reproduce the basic crescent eddy flow pattern and heat transfer characteristics (isotherms, temperature profiles, and Nusselt numbers) as described by Bishop, Yin *et al.* reasonably well within their respective ranges of validity, at least for air and silicone oils. Secondly, although the isotherms depend markedly on the boundary conditions, the basic crescent eddy flow pattern appears to be relatively insensitive to them. Thirdly, the average Nusselt number is relatively insensitive to the flow pattern. Fourthly, for sufficiently narrow gaps and sufficiently large Rayleigh or Grashof number, the nonlinear governing equations apparently admit two steady axisymmetric flow patterns (Caltagirone *et al.* 1980), a single-eddy pattern (the crescent eddy flow pattern), and a multiple-eddy flow pattern, in which a weak, counter-rotating eddy appears at the top of the annulus adjacent to the vertical axis and a second weak eddy may appear at the bottom of the annulus. It remains unresolved whether or not the multicellular flow is observable.

The linear stability results presented here will determine the critical Grashof numbers and also the spatial and temporal nature of the bifurcated flow. To date only two analyses of the stability of the basic motion have been reported in the literature. Mojtabi & Caltagirone (1982) investigated the linear stability of the basic motion for infinite Prandtl number. They assumed that the instability sets in at the top of the annulus, thereby reducing the partial differential equations governing the disturbances to a coupled system of ordinary differential equations by neglecting the dependence on the latitudinal angle. Farmer, Douglass & Trogdon (1986) used linear theory to study the stability of the basic motion to infinitesimal, axisymmetric disturbances and determined a set of critical Grashof numbers and corresponding heat transfer rates for a range of Prandtl numbers and gap widths. Their study used

the Boussinesq approximation and an analytical representation of the basic motion determined by Wright & Douglass (1986), and assumed bifurcation to a steady, axisymmetric flow pattern at the critical Grashof number. An error in the basic motion for flows in which the temperature of the inner sphere is greater than that of the outer sphere caused the stability results and conclusions to be incorrect.

The present investigation provides linear stability results for natural convection in concentric spherical annulus enclosures, in which the inner sphere has a higher temperature than the outer sphere. The disturbances in the present investigation are fully three-dimensional, and no assumption is made regarding the temporal nature of the bifurcation other than to use an exponential time factor to produce an eigenvalue problem. In particular, no principle of exchange of stabilities is assumed to exist; in fact, the existence of such a principle for this problem depends on the value of the Prandtl number. The disturbances are expressed as full spectral expansions in terms of spherical harmonics and Chebyshev polynomials; truncating the expansions reduces the governing partial differential equations to a matrix eigenvalue problem. The matrix eigenvalue problem is solved using a modified tau method described by Gardner, Trogdon & Douglass (1989); the notable feature of this approximate method is that it eliminates the computation of spurious eigenmodes. Calculations are performed for Prandtl numbers of 0, 0.025 (corresponding to mercury at 20 °C), 0.1, and 0.4, and 0.7 (corresponding to air), and for radius ratios (the ratio of the inner sphere radius to the outer sphere radius) of 0.900 and 0.950.

We begin with a description of the equations governing the evolution of infinitesimal, non-axisymmetric disturbances to the steady, axisymmetric basic motion of a Boussinesq fluid contained in a narrow-gap spherical annulus with isothermal boundaries. Numerical convergence of the critical eigenvalues will be discussed, and the critical eigenvalues and eigenvectors will be used to display the temporal and spatial nature of the bifurcated flow in a neighbourhood of the critical Grashof number.

2. The stability problem

Two concentric spheres, the inner one with radius $\tilde{r}_i$ and the outer one of radius $\tilde{r}_o$, are fixed with respect to each other and to an inertial reference frame attached to the surface of a gravitating body such as the Earth. The gap between the two spheres is completely filled by a single Boussinesq fluid. The inner and outer spheres are maintained at constant and spatially uniform temperatures $\tilde{T}_i$ and $\tilde{T}_o$, respectively. The gravitational acceleration vector $\tilde{\boldsymbol{g}}$ acts along a fixed vertical diameter with constant magnitude, $\tilde{g}$, and not everywhere radially as in the spherical Rayleigh–Bénard problem. The geometry of this system is depicted in figure 1. We shall examine the stability of the resulting flows to small perturbations.

2.1. *The governing equations*

We introduce a spherical polar coordinate system $(\tilde{r}, \theta, \phi)$ with its origin at the common centre of the spheres (figure 1); $\tilde{r}$ is the dimensional radius, θ is the azimuthal angle, and ϕ is the longitudinal angle. Let $\tilde{V}$, $\tilde{T}$, and $\tilde{P}$ represent the dimensional fluid velocity, temperature, and pressure, respectively, and let $\tilde{t}$ represent time. The spatial domain of interest is the gap between the spheres. The boundary conditions are the fixed temperatures of each sphere, and the no-slip velocity condition on each sphere.

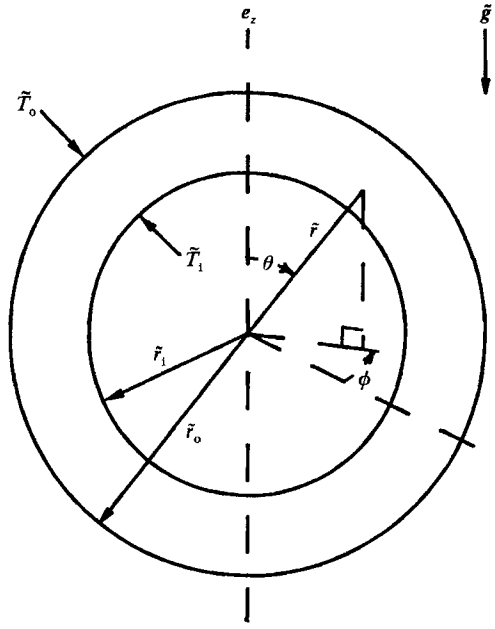

FIGURE 1. The geometry of the mathematical natural convection problem and the spherical polar coordinate system $(\tilde{r}, \theta, \phi)$.

We non-dimensionalize the equations governing the motion of a Newtonian fluid in the Boussinesq approximation using the scales $\Delta\tilde{r} = \tilde{r}_o - \tilde{r}_i$ (the gap width) for length, $\Delta\tilde{T} = |\tilde{T}_o - \tilde{T}_i|$ for temperature differences, $V^* = (\tilde{\alpha}_0 \Delta\tilde{T}\tilde{g}\Delta\tilde{r})^{\frac{1}{2}}$ (the rise velocity) for velocities, $P^* = \tilde{\rho}_0 (V^*)^2$ for pressure differences, and $\Delta\tilde{r}/V^*$ for time. $\tilde{\rho}_0$ is the fluid density and $\tilde{\alpha}_0$ is the coefficient of volumetric thermal expansion; the subscript 0 indicates evaluation at a convenient and appropriate reference state $(\tilde{T}_0, \tilde{P}_0)$. The corresponding dimensionless variables are written without tildes.

The dimensionless governing equations and boundary conditions are then

$$\nabla \cdot V = 0, \tag{1}$$

$$\frac{\partial V}{\partial t} + V \cdot \nabla V = -\nabla(P - P_s) + Te_z + \frac{1}{Gr^{\frac{1}{2}}} \nabla^2 V, \tag{2}$$

$$\frac{\partial T}{\partial t} + V \cdot \nabla T = \frac{1}{Pr\, Gr^{\frac{1}{2}}} \nabla^2 T, \tag{3}$$

$$T(r_i, \theta, \phi, t) = 1, \tag{4}$$

$$T(r_o, \theta, \phi, t) = 0, \tag{5}$$

$$V(r_i, \theta, \phi, t) = 0, \tag{6}$$

$$V(r_o, \theta, \phi, t) = 0. \tag{7}$$

Equations (1)–(3) formally comprise the Boussinesq approximation. $\tilde{P}_s$ is the hydrostatic pressure, defined by $\nabla\tilde{P}_s = -\tilde{\rho}_0 \tilde{g} e_z$; e_z is a unit vector in the upward vertical direction. Pr is the Prandtl number, and Gr is Grashof number (based on gap width), defined by $Pr = \tilde{\mu}_0 \tilde{c}_{p0}/\tilde{k}_0$ and $Gr = \tilde{\alpha}_0 \tilde{g} \Delta\tilde{T} (\Delta\tilde{r})^3 / \tilde{\nu}_0^2$. $\tilde{\mu}$ is the dynamic viscosity, $\tilde{c}_p$ is the specific heat capacity at constant pressure, $\tilde{k}$ is the thermal conductivity and $\tilde{\nu} = \tilde{\mu}/\tilde{\rho}$ is the kinematic viscosity. The stability parameter is the square root of Gr,

R. The radius ratio is $\eta = \tilde{r}_i/\tilde{r}_o$ and the dimensionless gap width is $\epsilon = 1-\eta$; in terms of ϵ and η, $r_i = \eta/\epsilon$ and $r_o = 1/\epsilon$. Equations (1)–(3) are valid for certain limits on $\Delta\tilde{r}$ and $\Delta\tilde{T}$, which depend on $\tilde{T}_0$, $\tilde{P}_0$ and the fluid properties. The expressions for the limits are given in Gardner (1988).

2.2. *The base flow solution*

In order to examine the entire stability curve, it is desirable to obtain a base flow solution which is valid for all dimensionless gap widths, Prandtl numbers, and Grashof numbers. Such solutions are available for limited ranges of η, Pr and Gr as described in the Introduction. We have selected, however, a solution which is valid for only small ϵ $(= 1-\eta)$ which is expressed as a truncated power series in ϵ (Wright & Douglass 1986). This solution is used here because it is known explicitly in terms of the independent spatial variables and parameters governing the flow. In addition, the solution has a known range of validity, and the results presented here for narrow gaps can, in some cases (viz., near the poles), be directly compared to the Rayleigh–Bénard problem having horizontal, isothermal, rigid–rigid boundaries.

The base flow solution is expressed as a stream function ψ and a temperature function T_0:

$$\psi(r,x) = (1-x^2)[\Gamma(r;R,Pr,\epsilon)+x\Delta(r;R,Pr,\epsilon)], \tag{8}$$

$$T_0(r,x) = T_1(r;R,Pr,\epsilon)+x[\Xi(r;R,Pr,\epsilon)+x\Omega(r;R,Pr,\epsilon)]. \tag{9}$$

x is the polar variable defined by

$$x = \cos\theta, \tag{10}$$

The functions Γ, Δ, T_1, Ξ, and Ω are nth-order expansions in ϵ (Gardner 1988). ψ and T_0 in (8) and (9) are valid for radius ratios η in the range $0.9 \leqslant \eta < 1$ and for values of R in the range

$$0 \leqslant R < \left[\frac{720}{(1-\eta)Pr}\right]^{\frac{1}{3}}, \tag{11}$$

when the expansion order is greater than or equal to eight. The validity of the stream and temperature functions given in (8) and (9) has been established by convergence studies in Wright (1984), and Wright & Douglass (1986).

Typical streamlines and isotherms for this base flow are shown in figure 2. A positive stream-function value represents a clockwise flow direction. In figure 2 the radial variable r has been mapped to the interval $[-1, 1]$ by the transformation

$$r = \frac{1}{2}\left[z+\frac{1+\eta}{1-\eta}\right]. \tag{12}$$

Because the gaps are narrow, the transformations (10) and (12) allow the streamlines and isotherms to be visualized in more detail than in the original variables.

2.3. *Derivation of the disturbance equations*

Let (V_0, T_0, P_0) represent a base flow, and let $(\hat{v}(r,x,\phi,t), \hat{T}(r,x,\phi,t), \hat{p}(r,x,\phi,t))$ be a disturbance to it. Substituting the sum $(V_0+\hat{v}, T_0+\hat{T}, P_0+\hat{p})$ into (1)–(7) and using the fact that (V_0, T_0, P_0) is a solution, we obtain

$$\nabla\cdot\hat{v} = 0, \tag{13}$$

$$\frac{\partial\hat{v}}{\partial t}+(V_0\cdot\nabla)\,\hat{v}+(\hat{v}\cdot\nabla)\;V_0+(\hat{v}\cdot\nabla)\,\hat{v} = -\nabla\hat{p}+\hat{T}e_z+\frac{1}{R}\nabla^2\hat{v}, \tag{14}$$

$$\frac{\partial\hat{T}}{\partial t}+(V_0\cdot\nabla)\,\hat{T}+(\hat{v}\cdot\nabla)\,T_0+(\hat{v}\cdot\nabla)\,\hat{T} = \frac{1}{RPr}\nabla^2\hat{T} \tag{15}$$

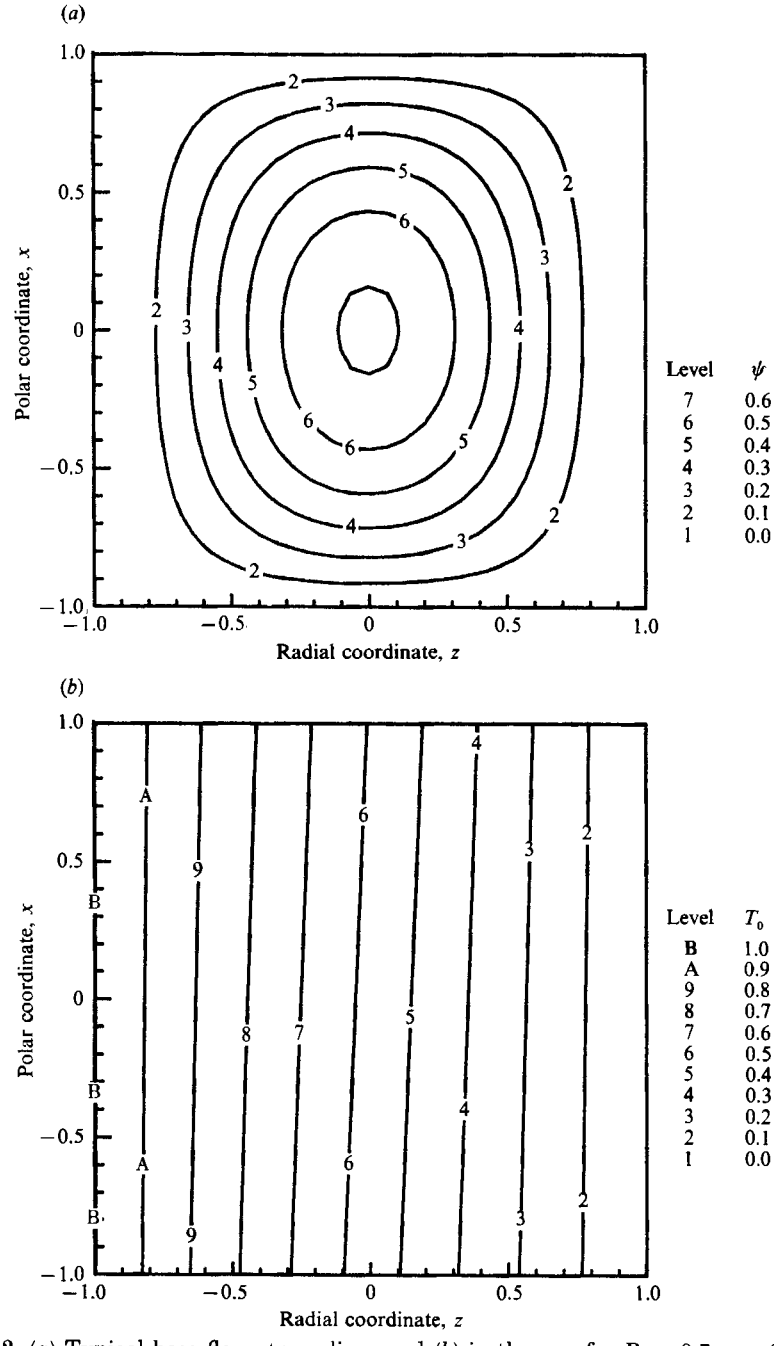

FIGURE 2. (*a*) Typical base flow streamlines and (*b*) isotherms, for $Pr = 0.7$, $\eta = 0.900$ and $R = 25$.

in the problem domain. We eliminate the pressure by taking the curl of (14), and obtain

$$\frac{\partial}{\partial t}\operatorname{curl}\hat{\boldsymbol{v}} = \operatorname{curl}(\hat{T}\boldsymbol{e}_z) + \operatorname{curl}[(\boldsymbol{V}_0\cdot\nabla)\hat{\boldsymbol{v}} + (\hat{\boldsymbol{v}}\cdot\nabla)\boldsymbol{V}_0 + (\hat{\boldsymbol{v}}\cdot\nabla)\hat{\boldsymbol{v}}] - \frac{1}{R}\operatorname{curl}^3\hat{\boldsymbol{v}}. \tag{16}$$

The boundary conditions are $\hat{T} = 0$ and $\hat{\boldsymbol{v}} = 0$ for $t \geqslant 0$. Equations (13), (15), and (16)

with these boundary conditions and some specified initial conditions are the equations governing the evolution of disturbances to the base flow.

2.4. *The linear stability problem*

Since $\hat{\boldsymbol{v}}$ is solenoidal, we can express the disturbance velocity $\hat{\boldsymbol{v}}$ as a sum of two other velocities which arise from the poloidal and toroidal potentials $\hat{\Phi}(r, x, \phi, t)$ and $\hat{\Psi}(r, x, \phi, t)$, respectively (see the Appendix). In the case of axisymmetric disturbances, $\hat{\Psi} \equiv 0$ and $\hat{\Phi}$ is related to the usual Stokes stream, function $\hat{\Lambda}$ by

$$\hat{\Lambda} = r(1-x^2)\frac{\partial \hat{\Phi}}{\partial x}. \tag{17}$$

The boundary conditions for $\hat{\Phi}$ and $\hat{\Psi}$ are obtained from the no-slip boundary condition on $\hat{\boldsymbol{v}}$: $\hat{\Phi} = \partial\hat{\Phi}/\partial r = \hat{\Psi} = 0$. $\hat{T} = 0$ on the boundaries since $T_0 + \hat{T}$ must satisfy the same boundary conditions as T_0. For an initial condition we can specify $\hat{\Phi}(r, x, \phi, 0)$, $\hat{\Psi}(r, x, \phi, 0)$, and $\hat{T}(r, x, \phi, 0)$ arbitrarily.

The disturbance equations can be written in the form

$$R\mathbf{M}\frac{\partial \hat{\boldsymbol{u}}}{\partial t} = \mathbf{L}(R, U)\,\hat{\boldsymbol{u}} + \mathbf{N}(R, U, \hat{\boldsymbol{u}}) \tag{18}$$

where $\mathbf{L}(r, U)$ and $\mathbf{N}(r, U, \hat{\boldsymbol{u}})$ are linear and bilinear operators, respectively. $U, \hat{\boldsymbol{u}}$, and $\mathbf{M}$ are given by

$$U = \begin{bmatrix} \psi \\ 0 \\ T_0 \end{bmatrix}, \quad \hat{\boldsymbol{u}} = \begin{bmatrix} \hat{\Phi} \\ \hat{\Psi} \\ \hat{T} \end{bmatrix}, \quad \mathbf{M} = \begin{bmatrix} \nabla^2\nabla_s^2 & 0 & 0 \\ 0 & \nabla_s^2 & 0 \\ 0 & 0 & Pr \end{bmatrix};$$

∇^2, ∇_s^2, $\mathbf{L}(R, U)$ and $\mathbf{N}$ are given in the Appendix. Initial bifurcation points of (18) are obtained by considering the linearized problem with an exponential time-dependence

$$\hat{\boldsymbol{u}} = \begin{bmatrix} \hat{\Phi} \\ \hat{\Psi} \\ \hat{T} \end{bmatrix} = \begin{bmatrix} \Phi \\ \Psi \\ T \end{bmatrix} \exp(\sigma t) = \boldsymbol{u}\exp(\sigma t); \tag{19}$$

the corresponding eigenvalue problem is

$$s\mathbf{M}\boldsymbol{u} = \mathbf{L}(R, U)\,\boldsymbol{u}, \quad s = \sigma R. \tag{20}$$

3. Numerical solution of the stability problem

To solve (20), we assume that the disturbance flow functions Φ, Ψ, and T may be expanded in a complete set of functions known as spherical harmonics. An approximate solution for them can be found as truncated series of the form

$$\Phi(r, x, \phi) \approx \sum_{l=1}^{N_p}\sum_{m=-1}^{m=1} g_{lm}(r)\,P_l^m(x)\exp(im\phi), \tag{21}$$

$$\Psi(r, x, \phi) \approx \sum_{l=1}^{N_p}\sum_{m=-1}^{m=1} f_{lm}(r)\,P_l^m(x)\exp(im\phi), \tag{22}$$

$$T(r, x, \phi) \approx \sum_{l=0}^{N_p-1}\sum_{m=-1}^{m=1} h_{lm}(r)\,P_l^m(x)\exp(im\phi). \tag{23}$$

The functions $g_{lm}(r)$, $f_{lm}(r)$, and $h_{lm}(r)$ represent the radial variation of the disturbance flow functions. The functions $P_l^m(x)$ are the associated Legendre functions.

We shall assume that, if the truncation order N_p is large enough to produce converged values of R and the critical eigenvalue σ_c, then it is large enough to produce at least a minimal trunction which preserves the bifurcation. Such a minimal truncation is the smallest such truncation that produces the same critical values for R and σ_c, and that will also produce the same sign (but not necessarily the same *magnitude*) for the first non-zero correction to R (Kloeden 1986). Thus the critical values and mode of the bifurcation are correctly produced by a minimal truncation.

Substituting (21)–(23) into (20) and using recursion relations for the associated Legendre functions and the orthogonality properties of the spherical harmonics produces a coupled, linear system of ordinary differential equations for the functions $g_{lm}(r)$, $f_{lm}(r)$, and $h_{lm}(r)$, which can be written in matrix form as

$$\boldsymbol{A}\boldsymbol{x} = s\boldsymbol{B}\boldsymbol{x}, \tag{24}$$

where the elements of the matrices $\boldsymbol{A}$ and $\boldsymbol{B}$ are differential operators and $\boldsymbol{x}$ is the eigenvector of functions $g_{lm}(r)$, $f_{lm}(r)$, and $h_{lm}(r)$. Since the base flow is axisymmetric, there is no coupling between modes with different wavenumbers. $\boldsymbol{B}$ is entirely real.

The system of equations (24) possesses an important symmetry property with respect to the wavenumber m. Note that for m less than zero we can write, for example,

$$\begin{aligned} f_{l,-|m|}(r)\,P_l^{-|m|}(x)\exp(-\mathrm{i}|m|\phi) &= f_{l,-|m|}(r)(-1)^{|m|}\frac{(l-|m|)!}{(l+|m|)!}P_l^{|m|}(x)\exp(-\mathrm{i}|m|\phi) \\ &= f'_{l,-|m|}(r)\,P_l^{|m|}(x)\exp(-\mathrm{i}|m|\phi), \end{aligned}$$

which, except for the minus sign in the exponential term, has exactly the same form as for m greater than zero. The only effect will be a change in sign in the terms arising from partial derivatives with respect to ϕ, which are imaginary. Thus the problem is represented in matrix form for m greater than zero by (24); the matrix problem for m less than zero can be represented by

$$\bar{\boldsymbol{A}}\bar{\boldsymbol{x}} = \bar{s}\boldsymbol{B}\bar{\boldsymbol{x}},$$

where the overbar indicates complex conjugation. That is, the eigenvalue for $-m$ is the complex conjugate of the eigenvalue for m, and the eigenvector for $-m$ is the complex conjugate of the eigenvector for m. Thus we need consider only non-negative values of m, and

$$f'_{l,-|m|}(r) = \bar{f}_{l,|m|}(r), \quad g'_{l,-|m|}(r) = \bar{g}_{l,|m|}(r), \quad h'_{l,-|m|}(r) = \bar{h}_{l,|m|}(r).$$

After some algebra we can then write

$$\Phi(r,x,\phi) = \sum_{l=1}^{N_p}\sum_{m=0}^{l}\frac{2}{c_m}[\mathrm{Re}\{g_{lm}(r)\}\cos(m\phi) - \mathrm{Im}\{g_{lm}(r)\}\sin(m\phi)]\,P_l^m(x), \tag{25}$$

$$\Psi(r,x,\phi) = \sum_{l=1}^{N_p}\sum_{m=0}^{l}\frac{2}{c_m}[\mathrm{Re}\{f_{lm}(r)\}\cos(m\phi) - \mathrm{Im}\{f_{lm}(r)\}\sin m\phi)]\,P_l^m(x), \tag{26}$$

$$T(r,x,\phi) = \sum_{l=0}^{N_p-1}\sum_{m=0}^{l}\frac{2}{c_m}[\mathrm{Re}\{h_{lm}(r)\}\cos(m\phi) - \mathrm{Im}\{h_{lm}(r)\}\sin(m\phi)]\,P_l^m(x), \tag{27}$$

where

$$c_m = \begin{cases} 2 & \text{for} \quad m = 0 \\ 1 & \text{for} \quad m > 0. \end{cases}$$

The solution algorithm for the stability problem is relatively straightforward. The objective is to obtain, for η and Pr fixed, the numbers

$$R_c = R(m_c;\, \eta,\, Pr) = \min_m \{R(m;\, \eta,\, Pr)\}$$

and

$$s_c = s(R_c;\, \eta,\, Pr), \quad \text{such that} \quad \mathrm{Re}\{s_c\} = 0.$$

Since the matrices $\boldsymbol{A}$ and $\boldsymbol{B}$ in (24) depend on η, Pr, and R, they must be updated whenever any of these parameters is changed.

The eigenvalue problem (24) is a boundary-value problem and can be solved numerically by various methods; the method used here is the modified Chebyshev-tau method (a full spectral method) of Gardner *et al.* (1989). This method is preferred over the usual Chebyshev-tau method (e.g. Gottlieb & Orszag 1977), in which spurious eigenvalues often arise (Orszag 1971). The modified tau method eliminates the computation of spurious eigenvalues.

The modified tau method is implemented by approximating the functions f_{lm}, g_{lm}, and h_{lm} as truncated series of Chebyshev polynomials of the form

$$f_{lm}(r) \approx \sum_{n=0}^{N_c} f_{lmn}\, T_n(z). \tag{28}$$

r is related to z via (12). $T_n(z)$ is the Chebyshev polynomial of order n. Using recursion relations for Chebyshev polynomials and their derivatives, and the orthogonal properties of the Chebyshev polynomials, a system of coupled, linear algebraic equations is produced from the system of differential equations. The resulting matrix eigenvalue problem is formally identical to (24), although the sizes and elements of $\boldsymbol{A}$ and $\boldsymbol{B}$ are different and the elements of the eigenvector $\boldsymbol{x}$ consist of the expansion coefficients f_{lmn}, etc., for $f_{lm}(r)$, $g_{lm}(r)$, and $h_{lm}(r)$. The symmetry property with respect to m is preserved under the approximation. A sequence of matrix operations then modifies the matrices $\boldsymbol{A}$ and $\boldsymbol{B}$ in such a way that spurious eigenvalues are not produced.

All the eigenvalues presented were computed using 64-bit arithmetic. A few test calculations were performed using 128-bit arithmetic, and the resulting eigenvalues agreed with those computed with 64-bit arithmetic to at least ten digits. All the critical eigenvalues reported have real parts whose absolute value is less than 1×10^{-3}.

4. The stability and bifurcation results

4.1. *Convergence of the critical eigenvalue and Grashof number*

The approximate eigenvalue problem has two truncation orders, N_p and N_c (see (25)–(28)). The truncation order N_c is related to the spatial resolution of the solution in the radial (i.e. z) direction, while the truncation order N_p is related to the spatial resolution of the solution on a sphere. The values of N_c and N_p required to adequately resolve the spatial structure of the solution depend on the scale of the significant structures in the solution. The smaller the scale of the significant structures, the larger N_c, or N_p, or both must be for the basis functions to resolve them.

The convergence of the eigenvalues as a function of N_c is indicated by the tau coefficients (Gardner *et al.* 1989). For a fixed value of N_p there will be in general eight N_p tau coefficients: four for each of the N_p g-functions, two for each of the N_p f-

Eigenvalue	$\|\tau\|$
$-27.663628342 \pm 86.627801020i$	2.314
$-32.515105196 \pm 69.977237447i$	0.9263
$-49.423985493 + 0.0000000000i$	0.4662
$-61.264575546 + 0.0000000000i$	2.707
$-108.57962079 + 0.0000000000i$	3.730
$-112.40441615 \pm 12.695568989i$	9.719

TABLE 1. The first nine eigenvalues with largest real part for $Pr = 0.7$, $\eta = 0.900$, $R = 200$, $m = 0$, $N_p = 6$, and $N_c = 21$

Truncation order, N_c	Eigenvalue	$\|\tau\|$
6	$-11.423670564 - 38.853023037i$	61.29
9	$-5.310040869\,3 - 14.061955770i$	16.60
12	$-5.270546347\,8 - 14.731373249i$	5.901
15	$-5.228333764\,3 - 14.723939951i$	1.248
18	$-5.228639208\,7 - 14.723375524i$	0.1329
21	$-5.228552528\,9 - 14.723261140i$	0.04459

TABLE 2. The effect of the Chebyshev truncation order N_c on the convergence of the eigenvalue with largest real part for $Pr = 0.7$, $\eta = 0.900$, $m = 2$, and $N_p = 6$

functions, and two for each of the N_p h-functions. We are not interested in the value of each tau coefficient, but only in some measure of whether the given eigenvalue is a good approximation to the true eigenvalue. Since, if the method is converging, all the tau coefficients for a given eigenvalue will ultimately decrease in magnitude as N_c increases, we examine here the behaviour of the sum of the absolute values of all the tau coefficients as a function of N_c.

The tau coefficients indicate only the relative degree of convergence of a given eigenvalue to the true eigenvalue, since they can be made arbitrarily large or small by scaling the eigenvectors from which they are computed. However, if the eigenvectors are scaled consistently, then the better approximations to the true eigenvalues will have smaller tau coefficients and the poorer approximations will have larger tau coefficients. This fact is illustrated by the eigenvalues and tau coefficients listed in table 1. Only the first nine eigenvalues and the corresponding tau coefficients are listed of the total of 228 eigenvalues for this case, for which the base flow is stable. Although the eigenvalue with largest real part does not have the smallest tau coefficient, it does not have a relatively small one and hence represents a good approximation to the true eigenvalue. In general, the eigenvalues with real parts that are larger in absolute value also have larger tau coefficients, indicating that these eigenvalues are poorer approximations to the corresponding true eigenvalues than those eigenvalues with real parts of smaller absolute value.

The eigenvalue with largest real part is given as a function of N_c in table 2, to illustrate the convergence as N_c increases. Convergence for other cases was similar. Although the value of N_p used in these calculations is small, its exact value is immaterial for demonstrating convergence as a function of N_c.

The effect of the number of spectral terms, N_p, on the convergence of the critical stability parameter, R_c, and the critical eigenvalue, s_c, is shown in figures 3 and 4. For

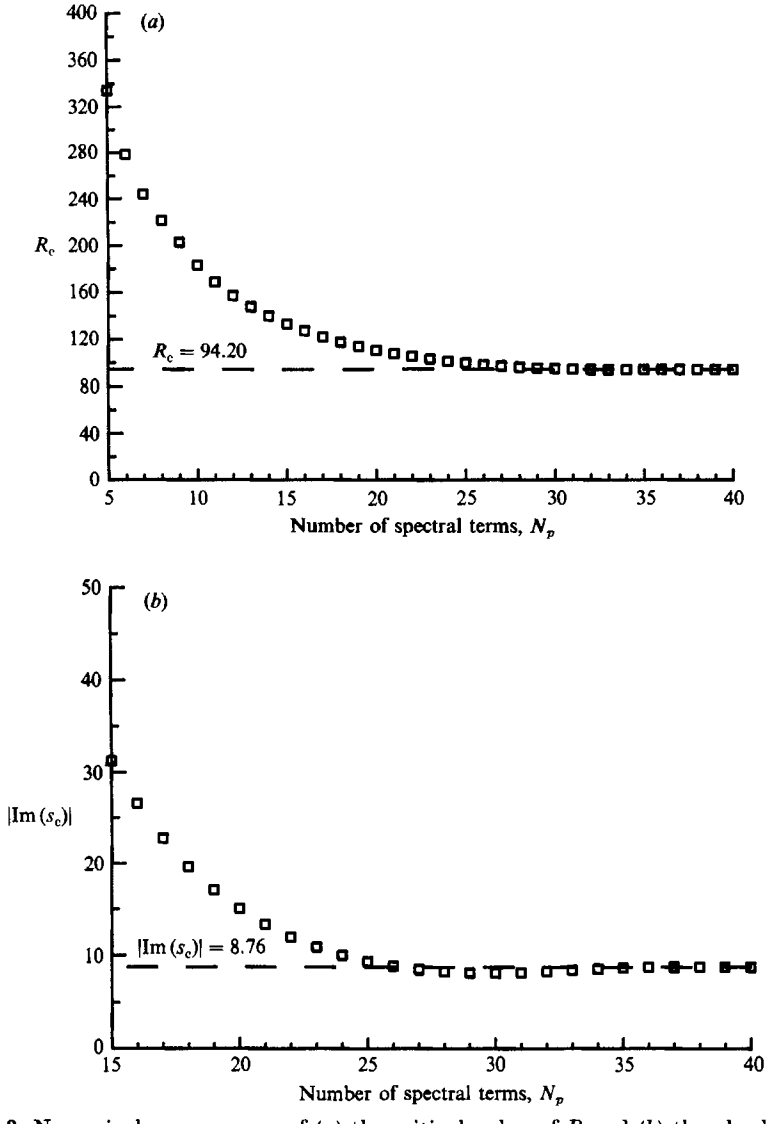

FIGURE 3. Numerical convergence of (*a*) the critical value of R and (*b*) the absolute value of the imaginary part of the critical eigenvalue, for $Pr = 0.1$, $\eta = 0.900$, $m = 0$, and $N_c = 12$.

a radius ratio of 0.900, both R_c and $|\mathrm{Im}\{s_c\}|$ have converged numerically for $N_p = 40$ (figure 3), to at least four and three digits, respectively (table 3). For a radius ratio of 0.950, neither R_c nor $|\mathrm{Im}\{s_c\}|$ has converged numerically for $N_p = 40$ (figure 4), and the epsilon algorithm (MacDonald 1964) was used to predict the converged values. (The epsilon algorithm provides a mechanism for estimating the converged value for a sequence of equally-spaced partial sums of a series. It works most effectively on monotonically increasing or decreasing sequences.)

These results indicate that the scale of the significant structures in the flow is smaller on a sphere than in the radial direction. The scale decreases as the radius ratio increases, since the value of N_p needed to obtain convergence increases as the relative gap width decreases. An estimate of the angular scale of the significant structures is π/N_o, where N_o is one plus the number of zeros in the associated

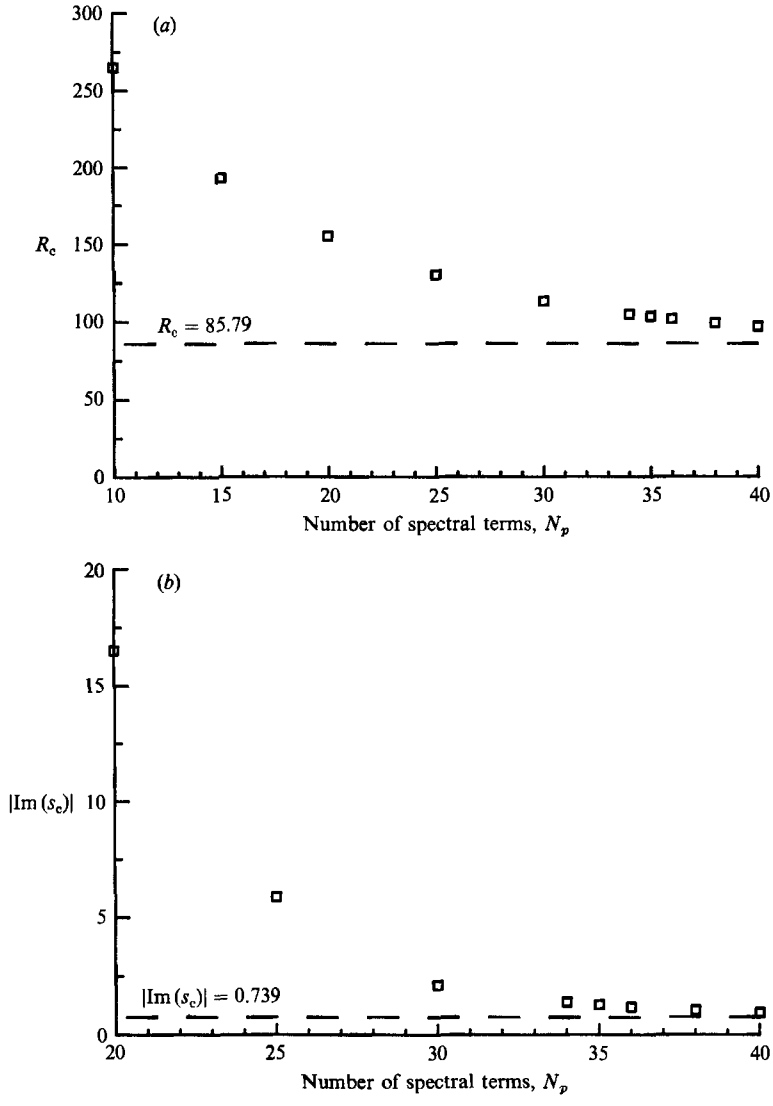

FIGURE 4. Numerical convergence of (*a*) the critical value of R and (*b*) the absolute value of the imaginary part of the critical eigenvalue, for $Pr = 0.1$, $\eta = 0.950$, $m = 0$, and $N_c = 12$.

Truncation order, N_p	R	$\lvert\mathrm{Im}\{s_c\}\rvert$
25	99.3699	9.34889
30	94.7810	8.13516
35	94.0901	8.67854
36	94.1470	8.74539
37	94.1858	8.76718
38	94.2001	8.76633
39	94.2020	8.76174
40	94.2013	8.75970

TABLE 3. The effect of the spectral truncation order N_p on the convergence of the eigenvalue with largest real part for $Pr = 0.1$, $\eta = 0.900$, $m = 0$, and $N_c = 12$

$Pr = 0.1$, $m = 0$	$Pr = 0.7$, $m = 2$
$R_c = 94.2013$	$R_c = 51.2960$
$0.000 \pm 8.75970i$	$0.000 + 0.00000i$
$-3.50403 \pm 7.50017i$	$-1.70676 + 0.00000i$
$-6.77380 \pm 6.31295i$	$-3.66579 + 0.00000i$
$-9.43722 \pm 5.50280i$	$-5.74716 + 0.00000i$
$-10.94775 \pm 3.75490i$	$-7.82333 + 0.00000i$
	$-9.86561 + 0.00000i$
	$-11.10902 + 0.00000i$
	$-11.57726 \pm 0.82199i$
	$-11.74836 + 0.00000i$

TABLE 4. The isolation of the critical eigenvalue for $\eta = 0.900$, $N_p = 40$, and $N_c = 12$. (The first ten eigenvalues for two cases.)

			$\eta = 0.900$[a]			
Pr	R_c	$\lvert\mathrm{Im}\{s_c\}\rvert$	m_c	Ra_c	Nu_c	$d\xi/dR$
0.000	108.704	26.868	0	—	1.1111	0.67
0.025	103.974	9.0164	0	270.3	1.1114	0.80
0.100	94.2013	8.7597	0	887.4	1.1140	0.80
0.250	86.3916	11.359	0	1886	1.1240	0.64
0.300	85.6993	11.896	0	2203	1.1288	0.59
0.305	85.6829	11.977	0	2239	1.1294	0.59
0.310	84.7601	0	0[b]	2227	1.1292	0.38
0.325	81.0881	0	0[b]	2137	1.1278	0.44
0.350	76.3451	0	0[b]	2040	1.1263	0.46
0.400	69.7370	0	0[b]	1945	1.1249	0.51
0.700	51.2960	0	2	1842	1.1235	0.60
			$\eta = 0.950$[c]			
Pr	R_c	$\lvert\mathrm{Im}\{s_c\}\rvert$	m_c	Ra_c	Nu_c	$d\xi/dR$[d]
0.000	98.1336	2.76232	0	—	1.0526	0.78
0.025	97.6485	1.51562	0	238.4	1.0527	0.80
0.100	85.7918	0.73855	0	736.0	1.0531	0.78
0.340	91.1904	0	0	2827	1.0599	0.34
0.400	79.7877	0	0[b]	2546	1.0585	0.31
0.700	53.0555	0	0[b]	1970	1.0562	0.35

[a] Critical values computed using values from $N_p = 40$ and $N_c = 12$.
[b] The critical wavenumber is two; the values reported are for $m = 0$.
[c] Critical values computed by the epsilon algorithm with $N_c = 12$.
[d] Computed using values from $N_p = 40$.

TABLE 5. The critical value of R, the critical eigenvalue, the critical wavenumber, the critical Rayleigh number, the critical Nusselt number, and the strict crossing derivative for radius ratios of 0.900 and 0.950

Legendre function $P_{N_p}^{m_c}(x)$, in which m_c is the critical wavenumber. This scale estimates the smallest structure that can be resolved by a truncated series involving associated Legendre functions of lower index N_p and upper index m_c. The smallest angular scale which can be resolved here is 4.39°.

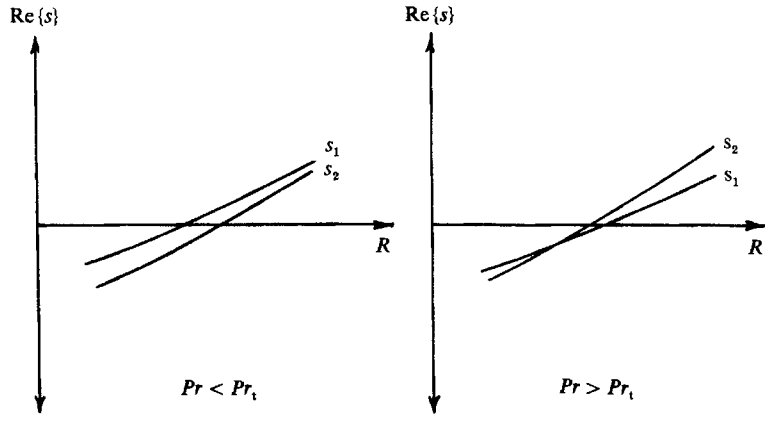

FIGURE 5. The change in critical eigenvalue at the transitional Prandtl number Pr_t.

$Pr = 0$		$Pr = 0.7$	
m	R_c	m	R_c
0	108.704	0	51.4834
1	108.758	1	51.3371
2	108.947	2	51.2960
3	109.248	3	51.3539
4	109.811		

TABLE 6. The determination of the critical wavenumber for $\eta = 0.900$, $N_p = 40$, and $N_c = 12$

4.2. *Linear stability of the base flow*

The isolation of the critical eigenvalues is illustrated by the data in table 4. The critical eigenvalue is isolated from the remaining ones, although the interval in R over which the eigenvalues are isolated may be quite small. A sufficient condition to ensure that a critical or bifurcation point has been identified is that the crossing of the critical eigenvalue be strict (i.e. $d\xi/dR \neq 0$, where $\xi = \mathrm{Re}\{s_c\}$). The strict crossing of the critical eigenvalue is shown by the values of $d\xi/dR$ at criticality given in table 5; also listed are the critical values of R, s, m, Ra_c, the critical Rayleigh number, and Nu_c, the average Nusselt number at criticality on the inner sphere. The values of $d\xi/dR$ at criticality were computed using a finite-difference approximation and data from $N_p = 40$ and $N_c = 12$.

The non-zero value of $|\mathrm{Im}\{s_c\}|$ for $\eta = 0.900$ and for Prandtl numbers in the range $0 \leqslant Pr < 0.31$ (table 5) indicates a time-periodic bifurcation, since to leading order the disturbances are given by (19). For $Pr > 0.31$, $|\mathrm{Im}\{s_c\}|$ is zero and hence the disturbance is steady at criticality. A transitional Prandtl number Pr_t thus exists at which the mode of bifurcation changes from time-periodic to steady as the Prandtl number is increased. This change in bifurcation mode as Pr increases is the result of a change in the identity of the eigenvalue that becomes the critical one, rather than a monotonic decrease of $|\mathrm{Im}\{s_c\}|$ to zero for a given eigenvalue. That is, suppose that for Prandtl numbers less than Pr_t the eigenvalue s_1 has the largest real part, and the eigenvalue s_2 has the next largest real part. As the Prandtl number is increased through Pr_t, we find that eigenvalue s_2 has largest real part and eigenvalue s_1 has

next largest real part (figure 5). For a radius ratio of 0.900, $Pr_t = 0.31$. A similar behaviour is observed for a radius ratio of 0.950, for which $Pr_t = 0.34$.

For Prandtl numbers in the range $0 \leqslant Pr < Pr_t$ the critical wavenumber m_c is zero (table 6), so in this Prandtl-number range the bifurcation is axisymmetric. For Prandtl numbers greater than the transitional Prandtl number, the critical wavenumber is two (table 6), so that the bifurcation is non-axisymmetric in this range. Thus for Prandtl numbers less than the transitional value Pr_t the bifurcation is time-periodic and axisymmetric, while for Prandtl numbers greater than Pr_t the bifurcation is steady and non-axisymmetric.

For comparison with experimental and other numerical results, the critical Rayleigh number $Ra_c = R_c^2 Pr$ is included in table 5. Although no experimental data exist for radius ratios as large as 0.900, the values computed here for $Pr = 0.7$ compare well with the data presented in the flow map for air (figure 9). One expects in the limit $\eta \to 1$ to recover the classical Rayleigh–Bénard result. $Ra_c = 1708$ for horizontal, isothermal, rigid–rigid planes; however, this is strictly true only for $m = 0$. Since for $Pr = 0.7 > Pr_t$ we have $m_c = 2$, this limit may not be achieved. Further analysis is required to resolve this. If it is assumed that the disturbances are axisymmetric, as in Douglass *et al.* (1990), the data suggest that the classical limit is approached as $\eta \to 1$.

The average Nusselt number for the outer sphere Nu_o is

$$Nu_o = \frac{1}{4\pi}\int_0^{2\pi}\int_{-1}^{1} \left.\frac{\partial T_0}{\partial r}\right|_{r=r_o} \mathrm{d}x\,\mathrm{d}\phi = -\eta^2 Nu_i.$$

since there is no internal energy generation. The critical Nusselt number Nu_c is defined to be the value of Nu_i evaluated for the given values of Pr and η and the critical value of R. Using the base flow solution (9),

$$Nu_c = \left[\frac{\partial T_1}{\partial r} + \frac{1}{3}\frac{\partial \Omega}{\partial r}\right]_{r=r_i}$$

For a given radius ratio, Nu_c increases with increasing Prandtl number for the range $0 \leqslant Pr < Pr_t$, while for Prandtl numbers greater than Pr_t, Nu_c decreases (table 5). These changes are relatively small. Changes in the values of Nu_c with changes in radius ratio (for fixed Prandtl number) are also small, on the order of 6% or less. These results reflect the relative insensitivity of R_c to the radius ratio for the results presented here.

4.3. *The bifurcation of the base flow*

For Prandtl numbers less than the transitional Prandtl number Pr_t the bifurcation is time-periodic and axisymmetric. Axisymmetry allows us to take $\hat{\Psi} \equiv 0$ and to relate $\hat{\Phi}$ to a stream function (17); we can define a critical stream function $\hat{\Lambda}_c$ by

$$\hat{\Lambda}_c = r(1-x^2)\frac{\partial \hat{\Phi}_c}{\partial x}. \tag{29}$$

In (29) the $\hat{\Phi}_c$ is the component of $\hat{\Phi}$ for the critical wavenumber m_c. The critical component $\hat{T}_c$ of the disturbance temperature is defined similarly. As a first approximation, we can take $(\hat{\Phi}_c, \hat{\Psi}_c, \hat{T}_c)^T$ to be the eigenvector corresponding to the critical eigenvalue s_c, multiplied by the exponential time factor (19). Streamlines determined from the contours of (29) are illustrated in figures 6 and 7. For $\eta = 0.900$

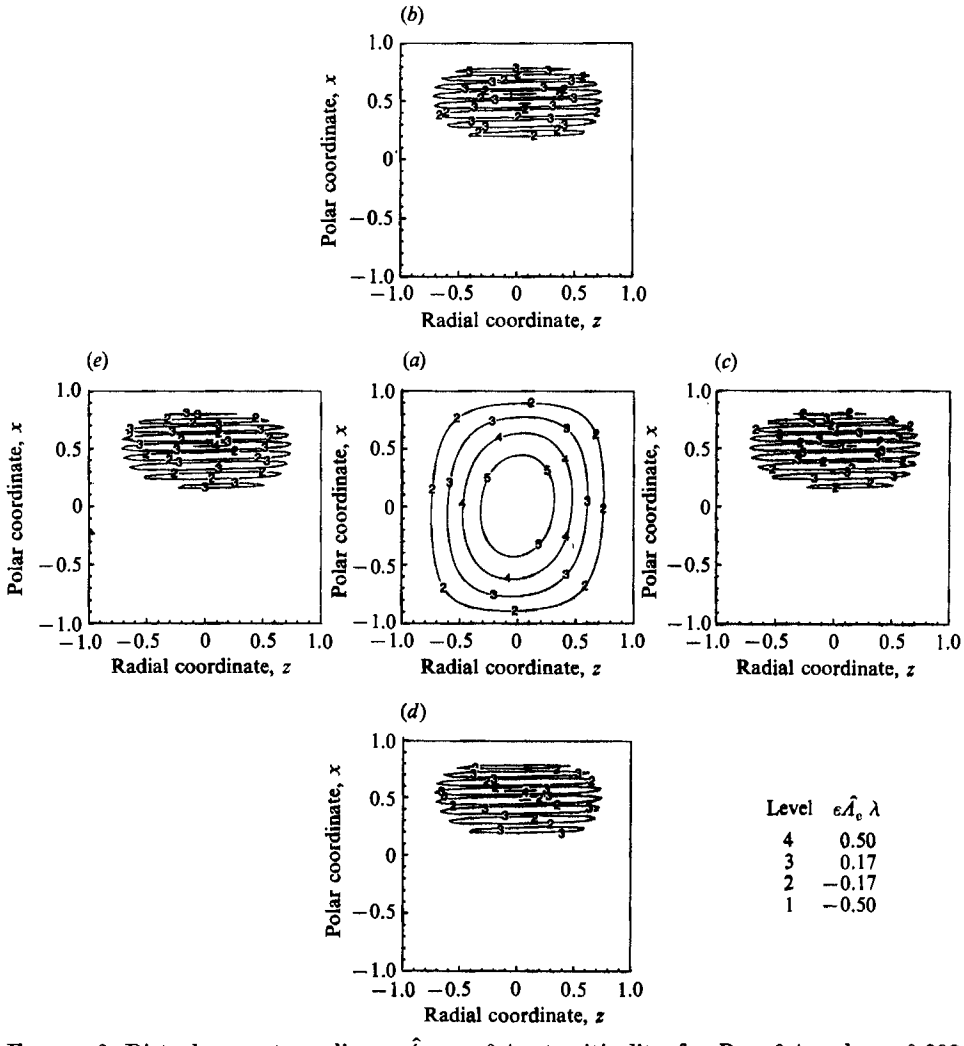

FIGURE 6. Disturbance streamlines $\epsilon\hat{A}_c$, $\epsilon = 0.1$, at criticality for $Pr = 0.1$ and $\eta = 0.900$. $R_c = 94.2013$, $m_c = 0$, $N_p = 40$, and $N_c = 12$. (*a*) Base flow streamlines, from (*b–e*) disturbance flow streamlines at times $w = \omega_0 t = 0, \frac{1}{2}\pi, \pi$ and $\frac{3}{2}\pi$ respectively. (All plots have the same axes. A positive stream function value indicates a clockwise flow direction. The scale is for the disturbance streamlines, $\epsilon\hat{A}_c$, only.)

and $Pr = 0.1$, the instability sets in as a cluster of toroidal rolls centred at approximately $x = 0.5$ (30° from the top of the annulus). Disturbance streamlines are shown in figure 7 for $\eta = 0.900$ and $Pr = 0$; the cluster of rolls is centred at $x \approx -0.1$ (96° from the top of the annulus).

This behaviour parallels that of the critical disturbances in the analogous stability problem in concentric horizontal cylinders (Walton 1980). For the concentric cylinders, the critical disturbance appears at $x = 0$ when $Pr = 0$. The polar coordinate at which the disturbance sets in increases with Prandtl number until, at a transitional Prandtl number of 0.24 (for 'narrow gaps'), the disturbance sets in at $x = 1$, and does so for all greater Prandtl numbers. This is quite similar to the behaviour observed here, where $(\eta, Pr_t) = (0.900, 0.31)$ and $(0.950, 0.34)$.

For Prandtl numbers greater than Pr_t the bifurcation is steady and non-

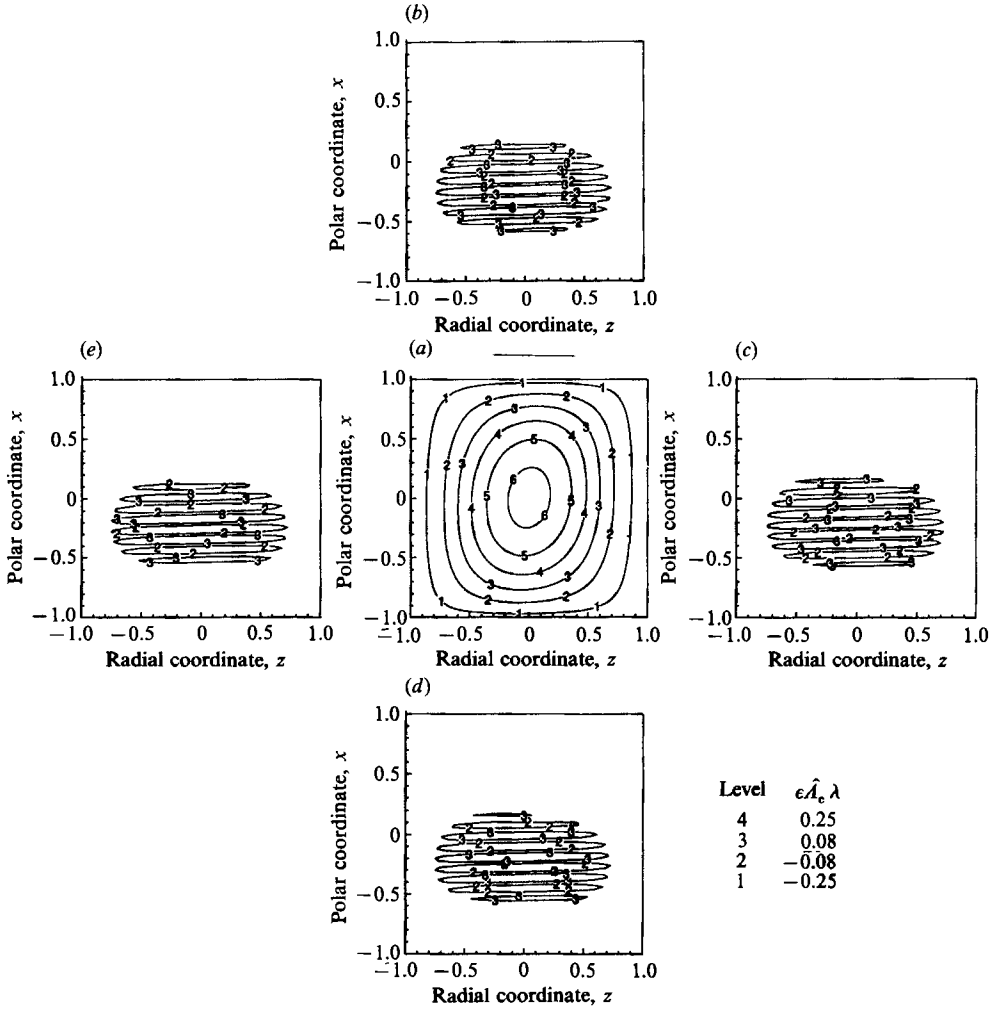

FIGURE 7. Disturbance streamlines $\epsilon\hat{A}_c$, $\epsilon = 0.1$, at criticality for $Pr = 0$ and $\eta = 0.900$. $R_c = 108.704$, $m_c = 0$, $N_p = 40$, and $N_c = 12$. (*a*) Base flow streamlines, (*b–e*) disturbance flow streamlines at times $w = \omega_0 t = 0$, $\frac{1}{2}\pi$, π and $\frac{3}{2}\pi$ respectively. (All plots have the same axes. A positive stream function value indicates a clockwise flow direction. The scale is for the disturbance streamlines, $\epsilon\hat{A}_c$, only.)

axisymmetric. The non-axisymmetric nature of the bifurcation precludes the use of contours of a stream function to display the streamlines. We can obtain some insight into the nature of the disturbance flow, however, by examining components of the disturbance velocity. The critical disturbance velocity components $\hat{v}_{rc}, \hat{v}_{xc}$, and $\hat{v}_{\phi c}$ can be determined from the expressions for the disturbance velocities and the critical components of the disturbance poloidal and toroidal potentials $\hat{\Phi}_c$ and $\hat{\Psi}_c$:

$$\hat{v}_{rc} = \frac{1}{r}\sum_{l=M}^{N_p}\frac{2}{c_m}l(l+1)\left[\mathrm{Re}\{g_{lm}\}\cos(m\phi+\omega_0 t) - \mathrm{Im}\{g_{lm}\}\sin(m\phi+\omega_0 t)\right]P_l^m(x), \tag{30}$$

$$\hat{v}_{xc} = -\sum_{l=M}^{N_p}\frac{2}{c_m}\left\{\frac{1}{r}\frac{\partial}{\partial r}\left[\mathrm{Re}\{rg_{lm}\}\cos(m\phi+\omega_0 t) - \mathrm{Im}\{rg_{lm}\}\sin(m\phi+\omega_0 t)\right]P_l^{m+1}(x)\right.$$
$$\left. + \frac{mP_l^m(x)}{r(1-x_2)^{\frac{1}{2}}}\left[\mathrm{Re}\{f_{lm}\}\sin(m\phi+\omega_0 t) + \mathrm{Im}\{f_{lm}\}\cos(m\phi+\omega_0 t)\right]\right\},$$

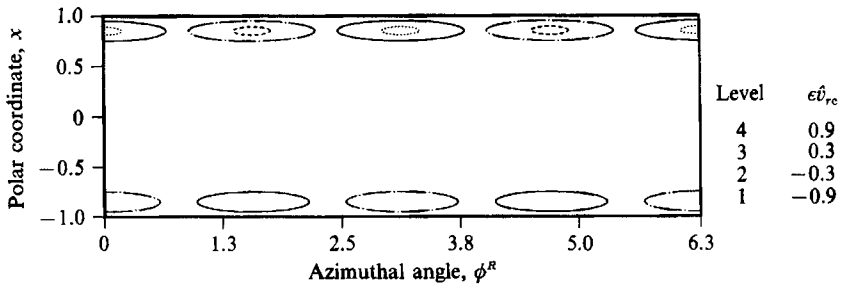

FIGURE 8. Disturbance radial velocity contours $\epsilon\hat{v}_{rc}$, $\epsilon = 0.1$, on the sphere $z = 0$ at criticality for $Pr = 0.7$ and $\eta = 0.900$. $R_c = 51.2960$, $m_c = 2$, $N_p = 40$, and $N_c = 12$.

$$\hat{v}_{\phi c} = -\sum_{l=M}^{N_p} \frac{2}{c_m}\left\{\frac{mP_l^m(x)}{r(1-x^2)}\frac{\partial}{\partial r}[\mathrm{Re}\{rg_{lm}\}\sin(m\phi+\omega_0 t)+\mathrm{Im}\{rg_{lm}\}\cos(m\phi+\omega_0 t)]\right.$$
$$\left.-[\mathrm{Re}\{f_{lm}\}\cos(m\phi+\omega_0 t)-\mathrm{Im}\{f_{lm}\}\sin(m\phi+\omega_0 t)]P_l^{m+1}(x)\right\},$$

where $M = \max\{m, l\}$, $\omega_0 = \mathrm{Im}\{\sigma_c\} = 0$, and $m = m_c$.

To explore the nature of the disturbance flow field, the disturbance radial velocity (30) was computed for Prandtl number 0.7 and radius ratio 0.900 at criticality. Contours of $\hat{v}_{rc}$ on the sphere $z = 0$ are presented in figure 8. In this figure, the upper and lower edges correspond to the north and south poles, $x = 1$ and $x = -1$, respectively, of the sphere $z = 0$. The disturbance flow includes a cluster of four cells arranged symmetrically around each pole of the annulus. In each cluster, if the flow in one cell is radially outward, the flow in the two adjoining cells is radially inward, so that the flow alternates in the radial direction from one cell to either adjacent one.

5. Summary of the problem and the results

The linear stability of natural convection flow of a Boussinesq fluid in a narrow-gap concentric spherical annulus has been explored, for the case where the inner sphere has a higher temperature than the outer sphere. The essential parameters for the problem are the radius ratio, the Prandtl number, and the Grashof number; the square root of the Grashof number, R, is the stability parameter. Critical Grashof numbers, critical eigenvalues, and critical wavenumbers were determined for Prandtl numbers ranging from zero to 0.7, and for radius ratios of 0.900 and 0.950. The convergence of the critical eigenvalues as functions of the truncation orders N_c and N_p was thoroughly explored. N_c was fixed at twelve. A value of $N_p = 40$ was necessary to ensure convergence for a radius ratio of 0.900. For a radius ratio of 0.950, numerical convergence required $N_p > 40$, and the epsilon algorithm was used to estimate the converged values.

For a radius ratio of 0.900, critical values of the stability parameter R ranged from 108.704 for a Prandtl number Pr of zero to 51.2960 for $Pr = 0.7$. For a radius ratio of 0.950, critical values of r ranged from 98.1336 for $Pr = 0$ to 53.0555 for $Pr = 0.7$. For a given radius ratio, there is a transitional value of the Prandtl number, Pr_t, at which the mode of the bifurcation changes. For $Pr < Pr_t$ the bifurcation is time-periodic and axisymmetric, while for $Pr > Pr_t$ the bifurcation is steady and non-axisymmetric, with wavenumber two. This transition is the result of a change in

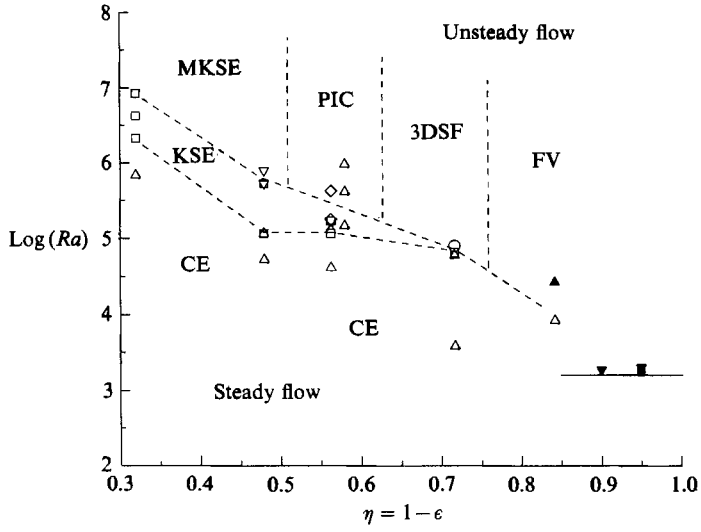

FIGURE 9. Comparison of the critical Rayleigh numbers for Prandtl number 0.7 (▼) ($N_p = 40$, $N_c = 12$) with experimental data for air: CE, crescent eddy; KSE, kidney-shaped eddy; MKSE, modified kidney-shaped eddy; PIC, periodic internal contracting eddy; 3DSF, three-dimensional steady flow; FV, falling vortex (nomenclature and data after Bishop *et al.* 1964 *a*, *b* and Yin *et al.* 1973); ■, from Douglass *et al.* (1990) for $N_p = 75$ and $N_c = 8$. The solid horizontal line is the Rayleigh–Bénard limit $Ra_c = 1708$ for horizontal, isothermal, rigid–rigid planes.

which eigenvalue is the critical one. Pr_t is 0.31 for a radius ratio of 0.900 and 0.34 for a radius ratio of 0.950. The existence of a transitional Prandtl number resembles the existence of a similar Prandtl number for the analogous problem in horizontal, concentric cylinders (Walton 1980).

A first approximation to the bifurcated flow was obtained using the eigenvector corresponding to the critical eigenvalue. For Prandtl numbers less than Pr_t, streamlines reveal that the critical disturbance is composed of a cluster of toroidal eddies that appear in the upper portion of the annulus. The eddies alternate in direction of rotation, and apparently remain fixed in location, but pulsate in strength with time. The location of the cluster moves toward the top of the annulus as the Prandtl number increases.

For Prandtl numbers greater than Pr_t, the disturbance radial velocity component was plotted for an imaginary spherical shell midway between the boundary spheres and concentric with them. This plot reveals that the disturbance flow possesses four regions clustered around each pole of the annulus where the velocity is alternately radially outward and radially inward, from one region to the adjacent ones.

Critical Rayleigh numbers Ra_c for Prandtl number 0.7 and radius ratios 0.900 and 0.950 compare favourably with extrapolated experimental results for air (figure 9). The computed bifurcation for Prandtl number 0.7 and narrow gaps is steady and non-axisymmetric, while the experimental data suggest that this bifurcation might be unsteady and axisymmetric (as is observed for Prandtl numbers less than Pr_t). The existence of the transitional Prandtl number may account for this, if $Pr = 0.7$ is less than the transitional Prandtl number for radius ratios where experimental data is available.

The critical Rayleigh number $Ra_c = 1842$ for $Pr = 0.7$ and $\eta = 0.900$ compares

favourably with the value of $Ra_c = 2350$ computed by Mojtabi & Caltagirone (1982) for concentric spheres with $\eta = 0.83$ and an infinite Prandtl number, assuming the disturbance sets in at the top of the annulus. It also compares favourably with the value $Ra_c = 1733$ computed by Walton (1980) for axisymmetric disturbances to natural convection flow in horizontal, concentric cylinders. Walton reports a transitional Prandtl number of ~ 0.24 (but reports no variation with η) and an expansion

$$Ra_c = Ra_0 + (1-\eta)Ra_1$$

for which the limit $\eta \to 1$ is $Ra_c = 1708$, the same result as for the classical Rayleigh–Bénard problem with rigid–rigid, horizontal isothermal boundaries. The classical limit may not be attained in the problem investigated here because the critical wavenumber is two, and not zero.

We have thus found that there is a flow bifurcation for Prandtl number 0.7 that seems consistent with the extrapolated experimental results for air. The bifurcation has also been explored in a neighbourhood of the critical Grashof number for various Prandtl numbers from zero to 0.7 and for radius ratios of 0.900 and 0.950. A transitional Prandtl number, at which the bifurcation mode changes from unsteady and axisymmetric to steady and non-axisymmetric is shown to exist; the value of the transition Prandtl number is 0.31 for radius ratio 0.900 and 0.34 for radius ratio 0.950.

This material is based on work supported by the National Science Foundation under Grant No. CBT-8612427. In addition, this work was partially supported by the National Center for Supercomputing Applications at the University of Illinois at Urbana-Champaign, and utilized the CRAY 2 system there. Partial support was also provided by the Department of Mechanical Engineering and the College of Engineering and Technology of the University of Nebraska-Lincoln. This support is gratefully acknowledged.

Appendix

The disturbance velocity $\hat{\boldsymbol{v}}$ is solenoidal; hence it can be expressed as a sum of two other velocities which arise from the poloidal and toroidal potentials $\hat{\Phi}(r, x, \phi, t)$ and $\hat{\Psi}(r, x, \phi, t)$, respectively (Chandrasekhar 1961; Sherman 1968; Warner 1972; Joseph 1976): $\hat{\boldsymbol{v}} = \hat{\boldsymbol{v}}_1 + \boldsymbol{v}_2$, where $\hat{\boldsymbol{v}}_1 = \mathrm{curl}^2(\boldsymbol{r}\hat{\Phi})$ and $\hat{\boldsymbol{v}}_2 = \mathrm{curl}(\boldsymbol{r}\hat{\Psi})$. The potentials are unique to within an additive function of r. To express (15) and (16) in terms of $\hat{\Phi}$ and $\hat{\Psi}$, we substitute them directly into (15), and apply the operators $\boldsymbol{r}\cdot\mathrm{curl}$ and $\boldsymbol{r}\cdot\mathrm{curl}^2$ to (16) to obtain the nonlinear equations for the evolution of the disturbance flow:

$$\frac{\partial}{\partial t}\nabla^2\nabla_s^2\hat{\Phi} = -\frac{1}{r}\nabla_s^2(\hat{T}x) + \mathscr{K}\left(\frac{\partial}{\partial x}[(1-x^2)\hat{T}]\right) + \frac{1}{R}\nabla^4\nabla_s^2\hat{\Phi} - \frac{1}{r^2}\nabla_s^2\left[\frac{\partial\psi}{\partial r}\frac{\partial}{\partial x}\nabla^2\hat{\Phi}\right.$$

$$\left. + E^2(\psi)\frac{\partial}{\partial x}\mathscr{K}(\hat{\Phi})\right] + \frac{1}{r}\frac{\partial}{\partial r}\left[\frac{1}{r}\frac{\partial\psi}{\partial x}\nabla^2\nabla_s^2\hat{\Phi} + \frac{(1-x^2)}{r}\frac{\partial^2\psi}{\partial x^2}\frac{\partial}{\partial x}\nabla^2\hat{\Phi}\right]$$

$$+ \frac{1}{r}\frac{\partial}{\partial r}\left[\frac{1}{r}\frac{\partial}{\partial x}(E^2(\psi)\nabla_s^2\hat{\Phi})\right] + \frac{1}{r^2}\nabla_s^2\left[\frac{1}{1-x^2}\frac{\partial\psi}{\partial r}\frac{\partial}{\partial\phi}\mathscr{K}(\hat{\Psi}) + \frac{E^2(\psi)}{1-x^2}\frac{\partial\hat{\Psi}}{\partial\phi}\right]$$

$$-\frac{1}{r}\frac{\partial}{\partial r}\left[\frac{1}{r}\frac{\partial^2\psi}{\partial x^2}\frac{\partial}{\partial\phi}\mathscr{K}(\hat{\Psi})+\frac{1}{r(1-x^2)}\frac{\partial\psi}{\partial r}\frac{\partial}{\partial\phi}\nabla_s^2\hat{\Psi}\right]+\frac{1}{r}\nabla_s^2\left\{\mathscr{J}\left(\frac{\nabla^2\hat{\Phi},\hat{\Psi}}{x,\phi}\right)\right.$$
$$\left.+\mathscr{J}\left(\frac{\mathscr{K}(\hat{\Phi}),\mathscr{K}(\hat{\Psi})}{x,\phi}\right)-\mathscr{M}_1(\mathscr{K}(\hat{\Phi}),\nabla^2\hat{\Phi})-\mathscr{M}_1(\mathscr{K}(\hat{\Psi}),\hat{\Psi})\right\}$$
$$+\frac{1}{r}\frac{\partial}{\partial r}\left\{[\nabla^2(\nabla_s^2\hat{\Phi})]\nabla_s^2\hat{\Phi}+\mathscr{M}_1(\nabla^2\hat{\Phi},\nabla_s^2\hat{\Phi})+[\nabla_s^2\hat{\Psi}]\nabla_s^2\hat{\Psi}+\mathscr{M}_1(\hat{\Psi},\nabla_s^2\hat{\Psi})\right.$$
$$\left.+\mathscr{J}\left(\frac{\nabla_s^2\hat{\Phi},\mathscr{K}(\hat{\Psi})}{x,\phi}\right)+\mathscr{J}\left(\frac{\nabla_s^2\hat{\Psi},\mathscr{K}(\hat{\Phi})}{x,\phi}\right)\right\}, \tag{A 1}$$

$$\frac{\partial}{\partial t}\nabla_s^2\hat{\Psi}=-\frac{\partial\hat{T}}{\partial\phi}+\frac{1}{R}\nabla^2\nabla_s^2\hat{\Psi}+\left\{\frac{1}{r^2}(1-x^2)\frac{\partial^2\psi}{\partial x^2}\frac{\partial}{\partial x}\mathscr{K}(\hat{\Psi})+\frac{1}{r^2}\frac{\partial\psi}{\partial x}\mathscr{K}(\nabla_s^2\hat{\Psi})\right.$$
$$\left.-\frac{\partial}{\partial x}\left[\frac{1}{r^2}\frac{\partial\psi}{\partial r}\nabla_s^2\hat{\Psi}\right]+\frac{1}{r^2}\frac{\partial}{\partial\phi}\left[\frac{\partial^2\psi}{\partial x^2}\nabla^2\hat{\Phi}-\frac{E^2(\phi)}{1-x^2}\nabla_s^2\hat{\Phi}\right]\right\}$$
$$-\frac{1}{r}\left\{\mathscr{J}\left(\frac{\nabla^2\hat{\Phi},\nabla_s^2\hat{\Phi}}{x,\phi}\right)+\frac{\partial}{\partial x}\left[\nabla_s^2\hat{\Psi}\frac{\partial\hat{\Psi}}{\partial\phi}\right]+\frac{\partial}{\partial\phi}\left[\nabla_s^2\hat{\Psi}\frac{\partial\hat{\Psi}}{\partial x}\right]\right.$$
$$-(\nabla_s^2\hat{\Phi})\mathscr{K}(\nabla_s^2\hat{\Psi})-(\nabla_s^2\hat{\Psi})\mathscr{K}(\nabla_s^2\hat{\Phi})+\frac{2}{1-x^2}\nabla_s^2\hat{\Psi}\frac{\partial^2}{\partial\phi^2}\mathscr{K}(\hat{\Phi})$$
$$\left.-\mathscr{M}_1(\nabla_s^2\hat{\Phi},\mathscr{K}(\hat{\Psi}))-\mathscr{M}_2(\mathscr{K}(\hat{\Phi}),\nabla_s^2(\hat{\Psi}))\right\}, \tag{A 2}$$

$$\frac{\partial\hat{T}}{\partial t}=\frac{1}{RPr}\nabla^2\hat{T}+\frac{1}{r^2}\mathscr{J}\left(\frac{\hat{T},\psi}{r,x}\right)+\frac{1}{r}\frac{\partial T_0}{\partial r}\nabla_s^2\hat{\Phi}+\frac{1}{r}\frac{\partial T_0}{\partial x}\frac{\partial\hat{\Psi}}{\partial\phi}-\frac{(1-x^2)}{r}\frac{\partial T_0}{\partial x}\frac{\partial}{\partial x}[\mathscr{K}(\hat{\Phi})]$$
$$-\frac{1}{r}\nabla_s^2\hat{\Phi}\frac{\partial\hat{T}}{\partial r}+\frac{1}{r}\left\{(1-x^2)\frac{\partial}{\partial x}[\mathscr{K}(\hat{\Phi})]-\frac{\partial\hat{\Psi}}{\partial\phi}\right\}\frac{\partial\hat{T}}{\partial x}+\frac{1}{r}\left\{\frac{1}{1-x^2}\frac{\partial}{\partial\phi}\mathscr{K}(\hat{\Phi})+\frac{\partial\hat{\Psi}}{\partial x}\right\}\frac{\partial\hat{T}}{\partial\phi}. \tag{A 3}$$

The operators ∇^2, ∇_s^2, ∇^4, $\mathscr{K}$, $\mathscr{J}$, E^2, $\mathscr{M}_1$ and $\mathscr{M}_2$ are given by

$$\nabla^2(f)=\frac{1}{r^2}\frac{\partial}{\partial r}\left(r^2\frac{\partial f}{\partial r}\right)+\frac{1}{r^2}\nabla_s^2(f),\quad \nabla_s^2(f)=\frac{\partial}{\partial x}\left[(1-x^2)\frac{\partial f}{\partial x}\right]+\frac{1}{1-x^2}\frac{\partial^2 f}{\partial\phi^2},$$

$$\nabla^4(f)=\nabla^2(\nabla^2 f),\quad \mathscr{K}(f)=\frac{1}{r}\frac{\partial}{\partial r}(rf),$$

$$\mathscr{J}\left(\frac{f,g}{x,\phi}\right)=\frac{\partial f}{\partial x}\frac{\partial g}{\partial\phi}-\frac{\partial f}{\partial\phi}\frac{\partial g}{\partial x},\quad E^2(f)=\frac{\partial^2 f}{\partial r^2}+\frac{1-x^2}{r^2}\frac{\partial^2 f}{\partial x^2},$$

$$\mathscr{M}_1(f,g)=(1-x^2)\frac{\partial f}{\partial x}\frac{\partial g}{\partial x}+\frac{1}{1-x^2}\frac{\partial f}{\partial\phi}\frac{\partial g}{\partial\phi},\quad \mathscr{M}_2(f,g)=(1-x^2)\frac{\partial f}{\partial x}\frac{\partial g}{\partial x}-\frac{1}{1-x^2}\frac{\partial f}{\partial\phi}\frac{\partial g}{\partial\phi}.$$

These equations can be written in the form

$$R\mathbf{M}\frac{\partial\hat{\boldsymbol{u}}}{\partial t}=\mathbf{L}(R,U)\hat{\boldsymbol{u}}+\mathbf{N}(R,U,\hat{\boldsymbol{u}}) \tag{A 4}$$

where $\mathbf{L}$ and $\mathbf{N}$ are respectively linear and bilinear operators. Definitions of U and $\hat{u}$ are given in the text. The components of $\mathbf{L}$ and $\mathbf{N}$ are

$$\mathrm{L}_{11}(\cdot) = \nabla^4\nabla_s^2(\cdot) - \frac{R}{r^2}\nabla_s^2\left[\frac{\partial\psi}{\partial r}\frac{\partial}{\partial x}\nabla^2(\cdot) + E^2(\psi)\frac{\partial}{\partial x}\mathscr{K}(\cdot)\right]$$
$$+\frac{R}{r}\frac{\partial}{\partial r}\left[\frac{1}{r}\frac{\partial\psi}{\partial x}\nabla^2\nabla_s^2(\cdot) + \frac{(1-x^2)}{r}\frac{\partial^2\psi}{\partial x^2}\frac{\partial}{\partial x}\nabla^2(\cdot)\right] + \frac{R}{r}\frac{\partial}{\partial r}\left[\frac{1}{r}\frac{\partial}{\partial x}(E^2(\psi)\nabla_s^2(\cdot))\right],$$

$$\mathrm{L}_{12}(\cdot) = \frac{R}{r^2}\nabla_s^2\left[\frac{1}{1-x^2}\frac{\partial\psi}{\partial r}\frac{\partial}{\partial\phi}\mathscr{K}(\cdot) + \frac{E^2(\psi)}{1-x^2}\frac{\partial(\cdot)}{\partial\phi}\right]$$
$$-\frac{R}{r}\frac{\partial}{\partial r}\left[\frac{1}{r}\frac{\partial^2\psi}{\partial x^2}\frac{\partial}{\partial\phi}\mathscr{K}(\cdot) + \frac{1}{r(1-x^2)}\frac{\partial\psi}{\partial r}\frac{\partial}{\partial\phi}\nabla_s^2(\cdot)\right],$$

$$\mathrm{L}_{13}(\cdot) = -\frac{R}{r}\nabla_s^2((\cdot)x) + R\mathscr{K}\left(\frac{\partial}{\partial x}[(1-x^2)(\cdot)]\right),$$

$$\mathrm{L}_{21}(\cdot) = -\frac{R}{r^2}\frac{\partial}{\partial\phi}\left[\frac{\partial^2\psi}{\partial x^2}\nabla^2(\cdot) - \frac{E^2(\psi)}{1-x^2}\nabla_s^2(\cdot)\right],$$

$$\mathrm{L}_{22}(\cdot) = \nabla^2\nabla_s^2(\cdot) + R\left\{\frac{1}{r^2}(1-x^2)\frac{\partial^2\psi}{\partial x^2}\frac{\partial}{\partial x}\mathscr{K}(\cdot) + \frac{1}{r^2}\frac{\partial\psi}{\partial x}\mathscr{K}(\nabla_s^2(\cdot)) - \frac{\partial}{\partial x}\left[\frac{1}{r^2}\frac{\partial\psi}{\partial r}\nabla_s^2(\cdot)\right]\right\},$$

$$\mathrm{L}_{23}(\cdot) = -R\frac{\partial\hat{T}}{\partial\phi},$$

$$\mathrm{L}_{31}(\cdot) = \frac{RPr}{r}\frac{\partial T_0}{\partial r}\nabla_s^2(\cdot) - RPr\frac{(1-x^2)}{r}\frac{\partial T_0}{\partial x}\frac{\partial}{\partial x}[\mathscr{K}(\cdot)],$$

$$\mathrm{L}_{32}(\cdot) = \frac{RPr}{r}\frac{\partial T_0}{\partial x}\frac{\partial(\cdot)}{\partial\phi},$$

$$\mathrm{L}_{33}(\cdot) = \nabla^2(\cdot) + \frac{RPr}{r^2}\mathscr{J}\left(\frac{(\cdot),\psi}{r,x}\right),$$

$$\mathrm{N}_1 = \frac{R}{r}\nabla_s^2\left\{\mathscr{J}\left(\frac{\nabla^2\hat{\Phi},\hat{\Psi}}{x,\phi}\right) + \mathscr{J}\left(\frac{\mathscr{K}(\hat{\Phi}),\mathscr{K}(\hat{\Psi})}{x,\phi}\right) - \mathscr{M}_1(\mathscr{K}(\hat{\Phi}),\nabla^2\hat{\Phi}) - \mathscr{M}_1(\mathscr{K}(\hat{\Psi}),\hat{\Psi})\right\}$$
$$+\frac{R}{r}\frac{\partial}{\partial r}\left\{[\nabla^2(\nabla_s^2\hat{\Phi})]\nabla_s^2\hat{\Phi} + \mathscr{M}_1(\nabla^2\hat{\Phi},\nabla_s^2\hat{\Phi}) + [\nabla_s^2\hat{\Psi}]\nabla_s^2\hat{\Psi} + \mathscr{M}_1(\hat{\Psi},\nabla_s^2\hat{\Psi})\right.$$
$$\left.+\mathscr{J}\left(\frac{\nabla_s^2\hat{\Phi},\mathscr{K}(\hat{\Psi})}{x,\phi}\right) + \mathscr{J}\left(\frac{\nabla_s^2\hat{\Psi},\mathscr{K}(\hat{\Phi})}{x,\phi}\right)\right\},$$

$$\mathrm{N}_2 = -\frac{R}{r}\left\{\mathscr{J}\left(\frac{\nabla^2\hat{\Phi},\nabla_s^2\hat{\Phi}}{x,\phi}\right) + \frac{\partial}{\partial x}\left[\nabla_s^2\hat{\Psi}\frac{\partial\hat{\Psi}}{\partial\phi}\right] + \frac{\partial}{\partial\phi}\left[\nabla_s^2\hat{\Psi}\frac{\partial\hat{\Psi}}{\partial x}\right]\right.$$
$$-(\nabla_s^2\hat{\Phi})\mathscr{K}(\nabla_s^2\hat{\Psi}) - (\nabla_s^2\hat{\Psi})\mathscr{K}(\nabla_s^2\hat{\Phi}) + \frac{2}{1-x^2}\nabla_s^2\hat{\Psi}\frac{\partial^2}{\partial\phi^2}\mathscr{K}(\hat{\Phi})$$
$$\left.-\mathscr{M}_1(\nabla_s^2\hat{\Phi},\mathscr{K}(\hat{\Psi})) - \mathscr{M}_2(\mathscr{K}(\hat{\Phi}),\nabla_s^2(\hat{\Psi}))\right\},$$

$$\mathrm{N}_3 = RPr\left\{-\frac{1}{r}\nabla_s^2\hat{\Phi}\frac{\partial\hat{T}}{\partial r} + \frac{1}{r}\left\{(1-x^2)\frac{\partial}{\partial x}[\mathscr{K}(\hat{\Phi})] - \frac{\partial\hat{\Psi}}{\partial\phi}\right\}\frac{\partial\hat{T}}{\partial x}\right.$$
$$\left.+\frac{1}{r}\left\{\frac{1}{1-x^2}\frac{\partial}{\partial\phi}\mathscr{K}(\hat{\Phi}) + \frac{\partial\hat{\Psi}}{\partial x}\right\}\frac{\partial\hat{T}}{\partial\phi}\right\}.$$

Introducing the coordinate transformation (12) the problem domain and boundaries are now

$$\{(z, x, \phi): \quad -1 < z < 1, \quad -1 \leqslant x \leqslant 1, \quad 0 \leqslant \phi \leqslant 2\pi\}$$
$$\{(z, x, \phi): \quad z = -1, \quad -1 \leqslant x \leqslant 1, \quad 0 \leqslant \phi \leqslant 2\pi\}$$
$$\{(x, x, \phi): \quad z = +1, \quad -1 \leqslant x \leqslant 1, \quad 0 \leqslant \phi \leqslant 2\pi\}.$$

The equations are

$$\begin{aligned}\mathscr{D}_l^2(\mathscr{D}_l^2 - s)\, g_{lm} + \frac{(2l+1)(l-m)!}{2l(l+1)(l+m)!}\Bigg\{ & R \sum_{k=m}^{N_m}\left[\mathscr{G}_{7lkm}\frac{\mathrm{d}h_{km}}{\mathrm{d}z} + \mathscr{G}_{8lkm}\, h_{km}\right] \\ & + R^2 \sum_{k=M}^{N_p}\left[\mathscr{G}_{0lkm1}\frac{\mathrm{d}^2 f_{km}}{\mathrm{d}z^2} + \mathscr{G}_{1lkm1}\frac{\mathrm{d}f_{km}}{\mathrm{d}z} + \mathscr{G}_{2lkm1}\, f_{km}\right. \\ & \left. + \mathscr{G}_{3lkm1}\frac{\mathrm{d}}{\mathrm{d}z}\mathscr{D}_k^2 g_{km} + \mathscr{G}_{4lkm1}\mathscr{D}_k^2 g_{km} + \mathscr{G}_{5lkm1}\frac{\mathrm{d}g_{km}}{\mathrm{d}z} + \mathscr{G}_{6lkm1}\, g_{km}\right] \\ & + R^4 \sum_{k=M}^{N_p}\left[\mathscr{G}_{0lkm2}\frac{\mathrm{d}^2 f_{km}}{\mathrm{d}z^2} + \mathscr{G}_{1lkm2}\frac{\mathrm{d}f_{km}}{\mathrm{d}z} + \mathscr{G}_{2lkm2}\, f_{km}\right. \\ & \left.\left. + \mathscr{G}_{3lkm2}\frac{\mathrm{d}}{\mathrm{d}z}\mathscr{D}_k^2 g_{km} + \mathscr{G}_{4lkm2}\mathscr{D}_k^2 g_{km} + \mathscr{G}_{5lkm2}\frac{\mathrm{d}g_{km}}{\mathrm{d}z} + \mathscr{G}_{6lkm2}\, g_{km}\right]\right\} = 0 \quad \text{(A 4)}\end{aligned}$$

for $l = M, M+1, \ldots, N_p$ with m fixed;

$$\begin{aligned}(\mathscr{D}_l^2 - s) f_{km} + \frac{(2l+1)(l-m)!}{2l(l+1)(l+m)!}\Bigg\{ & R \sum_{k=m}^{N_m}\mathscr{F}_{6lkm}\, h_{km} + R^2 \sum_{k=m}^{N_m}\left[\mathscr{F}_{1lkm1}\frac{\mathrm{d}f_{km}}{\mathrm{d}z} + \mathscr{F}_{2lkm1}\, f_{km}\right. \\ & \left. + \mathscr{F}_{3lkm1}\frac{\mathrm{d}^2 g_{km}}{\mathrm{d}z^2} + \mathscr{F}_{4lkm1}\frac{\mathrm{d}g_{km}}{\mathrm{d}z} + \mathscr{F}_{5lkm1}\, g_{km}\right] + \mathrm{R}^4 \sum_{k=M}^{N_p}\left[\mathscr{F}_{1lkm2}\frac{\mathrm{d}f_{km}}{\mathrm{d}z} + \mathscr{F}_{2lkm2}\, f_{km}\right. \\ & \left.\left. + \mathscr{F}_{3lkm2}\frac{\mathrm{d}^2 g_{km}}{\mathrm{d}z^2} + \mathscr{F}_{4lkm2}\frac{\mathrm{d}g_{km}}{\mathrm{d}z} + \mathscr{F}_{5lkm2}\, g_{km}\right]\right\} = 0 \qquad \text{(A 5)}\end{aligned}$$

for $l = M, M+1, \ldots, N_p$ with m fixed;

$$\begin{aligned}(\mathscr{D}_l^2 - sPr)\, h_{lm} + \frac{(2l+1)(l-m)!\,Pr}{2(l+m)!}\Bigg\{ & R \sum_{k=M}^{N_p}\mathscr{H}_{3lkm0}\, g_{km} \\ & + R^2 \sum_{k=m}^{N_m}\left[\mathscr{H}_{4lkm1}\frac{\mathrm{d}h_{km}}{\mathrm{d}z} + \mathscr{H}_{5lkm1}\, h_{km}\right] \\ & + R^3 \sum_{k=M}^{N_p}\left[\mathscr{H}_{1lkm1}\, f_{km} + \mathscr{H}_{2lkm1}\frac{\mathrm{d}g_{km}}{\mathrm{d}z} + \mathscr{H}_{3lkm1}\, g_{km}\right] \\ & + R^4 \sum_{k=m}^{N_m}\left[\mathscr{H}_{4lkm2}\frac{\mathrm{d}h_{km}}{\mathrm{d}z} + \mathscr{H}_{5lkm2}\, h_{km}\right] \\ & \left. + R^5 \sum_{k=M}^{N_m}\left[\mathscr{H}_{1lkm2}\, f_{km} + \mathscr{H}_{2lkm2}\frac{\mathrm{d}g_{km}}{\mathrm{d}z} + \mathscr{H}_{3lkm2}\, g_{km}\right]\right\} = 0 \qquad \text{(A 6)}\end{aligned}$$

for $l = m, m+1, \ldots, N_m$ with m fixed; where $M = \max\{1, m\}$ and $N_m = N_p + m - M$. The operator $\mathscr{D}_l^2(\cdot)$ is defined by

$$\mathscr{D}_l^2(\cdot) = 4\frac{\mathrm{d}^2(\cdot)}{\mathrm{d}z^2} + \frac{4}{r(z)}\frac{\mathrm{d}(\cdot)}{\mathrm{d}z} - \frac{l(l+1)}{r(z)^2}(\cdot).$$

The functions $\mathscr{G}_{jlkmn}$, $\mathscr{F}_{jlkmn}$, and $\mathscr{H}_{jlkmn}$ are given in Gardner (1988). The boundary conditions become

$$g_{km}(\pm 1) = \frac{\mathrm{d}g_{km}}{\mathrm{d}z}(\pm 1) = f_{km}(\pm 1) = h_{km}(\pm 1) = 0 \tag{A 7}$$

$$l = 0, 1, \ldots, N_p, \quad m = -l, -l+1, \ldots, -1, 0, 1, 2, \ldots l.$$

The equations (A 4)–(A 6) with the boundary conditions (A 7) comprise a system of coupled, linear ordinary differential equations, whose solution yields the eigenvalue s and the corresponding eigenvector of functions g_{lm}, f_{lm}, and h_{lm}.

The functions f_{lm}, g_{lm}, and h_{lm} are approximated by truncated series of Chebyshev polynomials of the form (28). Using recursion relations for the Chebyshev polynomials and their derivatives, and the orthogonality property of the Chebyshev polynomials, a system of coupled, linear algebraic equations is obtained for the expansion coefficients f_{lmn}, g_{lmn}, and h_{lmn}. The coefficients in the equations involve integrals of the form

$$Q_{nlk}^{pmj} = \int_{-1}^{1} (1-x^2)^{\frac{1}{2}p} P_n^0(x) P_k^j(x) P_l^m(x) \, \mathrm{d}x,$$

where $P_n^0(x)$ is the usual Legendre polynomial of order n. These integrals were evaluated by means of a 64-point Gaussian quadrature.

REFERENCES

Astill, K. N., Leong, H. & Martorana, R. 1980 A numerical solution for natural convection in concentric spherical annuli. In *Natural Convection in Enclosures*, pp. 105–113. ASME.

Bishop, E. H., Kolflat, R. S., Mack, L. R. & Scanlan, J. A. 1964 *a* Convective heat transfer between concentric spheres. In *Proc. 1964 Heat Transfer and Fluid Mechanics Institute, UC Berkeley, CA, 10–12 June 1964* (ed. W. H. Giedt & S. Levy), pp. 69–80, Stanford University Press, Stanford, CA.

Bishop, E. H., Kolflat, R. S., Mack, L. R. & Scanlan, J. A. 1964 *b* Photographic studies of convective patterns between concentric spheres. *9th SPIE Technical Symp., Miami Beach, FL, 28 August 1964*, pp. 47–49.

Bishop, E. H., Mack, L. R. & Scanlan, J. A. 1966 Heat transfer by natural convection between concentric spheres. *Intl J. Heat Mass Transfer* **9**, 649–652.

Brown, R. J. 1967 Natural convection heat transfer between concentric spheres. Ph.D. dissertation, University of Texas, Austin.

Caltagirone, J.-P., Combarnous, M. & Mojtabi, A. 1980 Natural convection between two concentric spheres: transition toward a multicellular flow. *Numer. Heat Transfer* **3**, 107–114.

Chandrasekhar, S. 1961 *Hydrodynamic and Hydromagnetic Stability*, pp. 220–226, 622–625, Oxford University Press.

Douglass, R. W., TeBeest, K. G., Trogdon, S. A. & Gardner, D. R. 1990 Prandtl number effects on the stability of natural convection between spherical shells. *Intl J. Heat Transfer* (in press).

Farmer, M. T., Douglass, R. W. & Trogdon, S. A. 1986 The stability of natural convection in narrow-gap spherical annuli to axisymmetric disturbances. *Intl J. Heat Mass Transfer* **29**, 1575–1584.

Gardner, D. R. 1988 Linear stability and bifurcation of natural convection flows in narrow-gap, concentric spherical annulus enclosures. Ph.D. dissertation, University of Nebraska, Lincoln.

Gardner, D. R., Trogdon, S. A. & Douglass, R. W. 1989 A modified tau spectral method that eliminates spurious eigenvalues. *J. Comput. Phys.* **80**, 137–167.

Gottlieb, D. & Orszag, S. A. 1977 *Numerical Analysis of Spectral Methods: Theory and Application*, pp. 159–161. SIAM.

INGHAM, D. B. 1981 Heat transfer by natural convection between spheres and cylinders. *Numer. Heat Transfer* **4**, 53–67.

JOSEPH, D. D. 1976 *Stability of Fluid Motions I & II.* Springer.

KLOEDEN, P. E. 1986 Minimal truncated spectral systems which preserve bifurcations. *Z. Angew. Math. Mech.* **66**, 51–54.

MACDONALD, J. R. 1964 Accelerated convergence, divergence, iteration, extrapolation, and curve fitting. *J. Appl. Phys.* **35**, 3034–3041.

MACK, L. R. & HARDEE, H. C. 1968 Natural convection between concentric spheres at low Rayleigh numbers. *Intl J. Heat Mass Transfer* **11**, 387–396.

MOJTABI, A. & CALTAGIRONE, J.-P. 1982 Natural convection between two concentric spheres for high Prandtl number. *Proc. 7th Intl Heat Transfer Conf. Munich,* vol. 2, pp. 245–249.

NELSEN, J. M., & DOUGLASS, R. W. 1984 Non-uniform energy generation effects on natural convection in a spherical annulus enclosure. *J. Heat Mass Transfer* **27**, 1928–1932.

NELSEN, J., DOUGLASS, R. & ALEXANDER, D. 1982 Natural convection in a spherical annulus filled with heat generating fluid. *Proc. 7th Intl Heat Transfer Conf.,* vol. 2, pp. 171–176.

ORSZAG, S. A. 1971 Accurate solution of the Orr–Sommerfeld stability equation. *J. Fluid Mech.* **50**, 689–703.

SHERMAN, M. 1968 Toroidal and poloidal field representation for convective flow within a sphere. *Phys. Fluids* **11**, 1895–1900.

SINGH, S. N. & CHEN, J. 1980 Numerical solution for free convection between concentric spheres at moderate Grashof numbers. *Numer. Heat Transfer* **3**, 441–459.

SINGH, S. N. & ELLIOT, J. M. 1981 Natural convection between concentric spheres in a slightly-thermally stratified medium. *Intl J. Heat Mass Transfer* **24**, 395–406.

WALTON, I. C. 1980 The stability of free convection in a horizontal cylindrical annulus. *Q. J. Mech. Appl. Maths* **33**, 125–139.

WARNER, W. H. 1972 Poloidal and toroidal potentials for solenoidal fields. *Z. Angew. Math. Phys.* **23**, 221–230.

WRIGHT, J. L. 1984 Natural convective flow in narrow gap spherical annuli. M.S. thesis, University of Nebraska, Lincoln.

WRIGHT, J. L. & DOUGLASS, R. W. 1986 Natural convection in narrow-gap, spherical annuli. *Intl J. Heat Mass Transfer* **29**, 725–739.

YIN, S. H., POWE, R. E., SCANLAN, J. A. & BISHOP, E. H. 1973 Natural convective flow patterns in spherical annuli. *J. Heat Mass Transfer* **16**, 1785–1795.